

Hydrodynamic stagnation zones: A new play concept for the Llanos Basin, Colombia

Mark Person, David Butler, Carl W. Gable, Tomas Villamil, David Wavrek, and Daniel Schelling

ABSTRACT

Hydraulic heads from a calibrated, three-dimensional, constant-density, ground-water-flow model were used to compute Hubbert oil potentials and infer secondary petroleum migration directions within the Llanos Basin, Colombia. The oil potentials for the C7 reservoir show evidence of the development of two hydrodynamic stagnation zones. Hydrodynamic effects on secondary oil migration are greatest in the eastern Llanos Basin, where structural slopes are lowest and local hydraulic-head gradients drive ground-water flow westward down structural dip. The Rubiales field, a large oil reservoir within the eastern Llanos Basin with no structural closure, is located at the edge of one of these stagnation zones. This oil field hosts heavy oils (12° API) consistent with water washing and biodegradation. The best agreement between model results and field conditions occurred in an oil density of 12° API, suggesting that the Rubiales field position is in dynamic equilibrium with modern hydraulic and oil density conditions.

Cross sectional ground-water-flow models indicate that the most likely explanation of observed underpressures are caused by hydrodynamic effects associated with a topography-driven flow system. Late Miocene to present-day ground-water flow likely was an important factor in flushing marine connate porewaters from Tertiary reservoirs. Ground-water recharge along the western margin of the basin could help explain the observed low-temperature gradients (20°C/km). However, upward flow rates were not high enough to account for elevated temperature gradients of 50°C/km to the east.

AUTHORS

MARK PERSON ~ *New Mexico Tech, Department of Earth and Environmental Sciences, 801 Leroy Place, Socorro, New Mexico 87801; markaustinperson@gmail.com*

Mark Person received his Ph.D. from the Department of Earth and Planetary Sciences at the Johns Hopkins University in 1990. He is currently a professor of hydrogeology at New Mexico Tech in Socorro, New Mexico. He is a director of Petroleum Hydrodynamics International, LLC, and an editor of the journal *Geofluids*.

DAVID BUTLER ~ *New Mexico Tech, Department of Earth and Environmental Sciences, 801 Leroy Place, Socorro, New Mexico 87545; dbutler@nmt.edu*

David Butler received his B.S. degree in earth and environmental science from the New Mexico Institute of Mining and Technology in 2011. He is currently a master's student in hydrology at New Mexico Tech in Socorro, New Mexico. His interests include basin-scale ground-water modeling, geothermal exploration, and carbon sequestration.

CARL W. GABLE ~ *Earth and Environmental Science Division, Los Alamos National Laboratory, Los Alamos, New Mexico; gable@lanl.gov*

Carl W. Gable received his Ph.D. in geophysics from Harvard University in 1989. He is currently the group leader of the Computational Earth Sciences Group at Los Alamos National Laboratory. His research interests include mesh generation and model setup for geologic applications, computational hydrology, and computational geometry.

TOMAS VILLAMIL ~ *Grupo C and C Energía, Carrera 4 N 72 35 Piso 8-Bogota, Colombia; tvillamil@ccenergy.com.co*

Tomas Villamil received his B.S. degree in geology from the National University in Bogotá. He received a Ph.D. in geology from the University of Colorado at Boulder. He was a postdoctoral fellow at the University of Colorado and Dartmouth College. He started his career in Tectonic Analysis at Conoco in Houston. He was the exploration vice president of Ecopetrol, exploration manager for Lukoil, and currently is the executive vice president of exploration for C and C Energia Ltd.

Copyright ©2012. The American Association of Petroleum Geologists. All rights reserved.

Manuscript received February 3, 2011; provisional acceptance May 2, 2011; revised manuscript received July 14, 2011; final acceptance August 10, 2011.

DOI:10.1306/08101111019

DAVID WAVREK ~ *Petroleum Systems International Inc., Salt Lake City, Utah 84111; dwavrek@petroleumsystems.com*

David A. Wavrek is currently president of Petroleum Systems International, Inc., in Salt Lake City, Utah. He recently received the 2010 Scientist of the Year award from Rocky Mountain Association of Geologists for his contributions that integrate diverse disciplines in petroleum systems studies. He received his Ph.D. in geosciences from the University of Tulsa in Tulsa, Oklahoma.

DANIEL SCHELLING ~ *Structural Geology International Inc., Salt Lake City, Utah 84103; dschelling@comcast.net*

Daniel D. Schelling graduated with a B.A. degree from Harvard University in 1979. He received his Ph.D. from the University of Colorado in 1989. He is currently director of Structural Geology International, LLC, in Salt Lake City, Utah. He is actively involved in fieldwork and structural analysis of fold-thrust belt systems.

ACKNOWLEDGEMENTS

We thank John D. Bredehoeft, Stephen E. Ingebritsen, William D. DeMis, and Martin S. Appold for their review comments on this article. The AAPG Editor thanks the following reviewers for their work on this paper: Martin S. Appold, John D. Bredehoeft, William D. DeMis, and Stephen E. Ingebritsen.

INTRODUCTION

Oil exploration within the Llanos Basin, Colombia (Figure 1), is complicated by the presence of an active ground-water-flow system. The Llanos Basin is a foreland-type sedimentary basin that covers 73,000 mi² (189,069 km²) of eastern Colombia and contains as much as 17,000 ft (5183 m) of Mesozoic and Tertiary sediments that thin to the east to 3000 ft (914 m) (Figure 2). Pore fluids in many regions of the Llanos Basin are brackish to fresh (Villegas et al., 1994) (Figure 3B), suggesting that marine units have been partially or completely flushed. Fresh water decreases the potential for buoyancy-driven oil migration and can complicate geophysically derived reserve estimates because fresh water has a similar electrical conductivity to oil (Krieger et al., 1996). Active ground-water-flow systems can strip reservoir oils of light aromatic hydrocarbons (HCs) and promote biodegradation if temperatures are less than 80°C (Head et al., 2003; Zhang et al., 2005). Emplacement of fresh water into source rocks can also promote biogenic gas plays in shales (e.g., McIntosh and Walter, 2006; Schlegel et al., 2011). Some oil fields within the eastern Llanos Basin show varying degrees of biodegradation (Howell et al., 1984). Basin-scale ground-water-flow systems can also impact the position of the oil-water contact within reservoirs in continental terrains (Hubbert, 1953; DeMis, 1987, 1995; Bethke et al., 1991; Eisenberg, 1993; Berg et al., 1994; Eisenberg et al., 1994). Some oil fields within the Llanos Basin are reported to have tilted oil-water contacts (e.g., Cano Limon, Castilla, and Rubiales; Figure 1A) (T. Villemil, 2009, personal communication) that dip in the direction of the hydraulic gradient. The Rubiales oil field (Figure 1A) is enigmatic in that it appears to be hydrodynamically entrapped. It is situated along a structural monocline that has no apparent structural closure (Figure 1B). Both facies changes and hydrodynamic effects have been proposed as entrapment mechanisms (Gómez et al., 2009). Keeley and Arevalo (1994) note that ground-water flow in the vicinity of Rubiales is from the northeast and that ground water flows down structural dips.

Villegas et al. (1994) report pore-fluid pressures to be near hydrostatic except in the deepest parts of the basin, where some measurements are well below the hydrostatic pressure gradient line (by 400 psi [2.7 MPa] relative to the land surface; Figure 3E). The subhydrostatic pressures are associated with deeply buried sandstone reservoirs on the western margin of the basin, where low-density conditions exist (930 kg/m³) because of high temperatures. Variations in fluid density can impact ground-water-flow directions (Bachu, 1995). However,

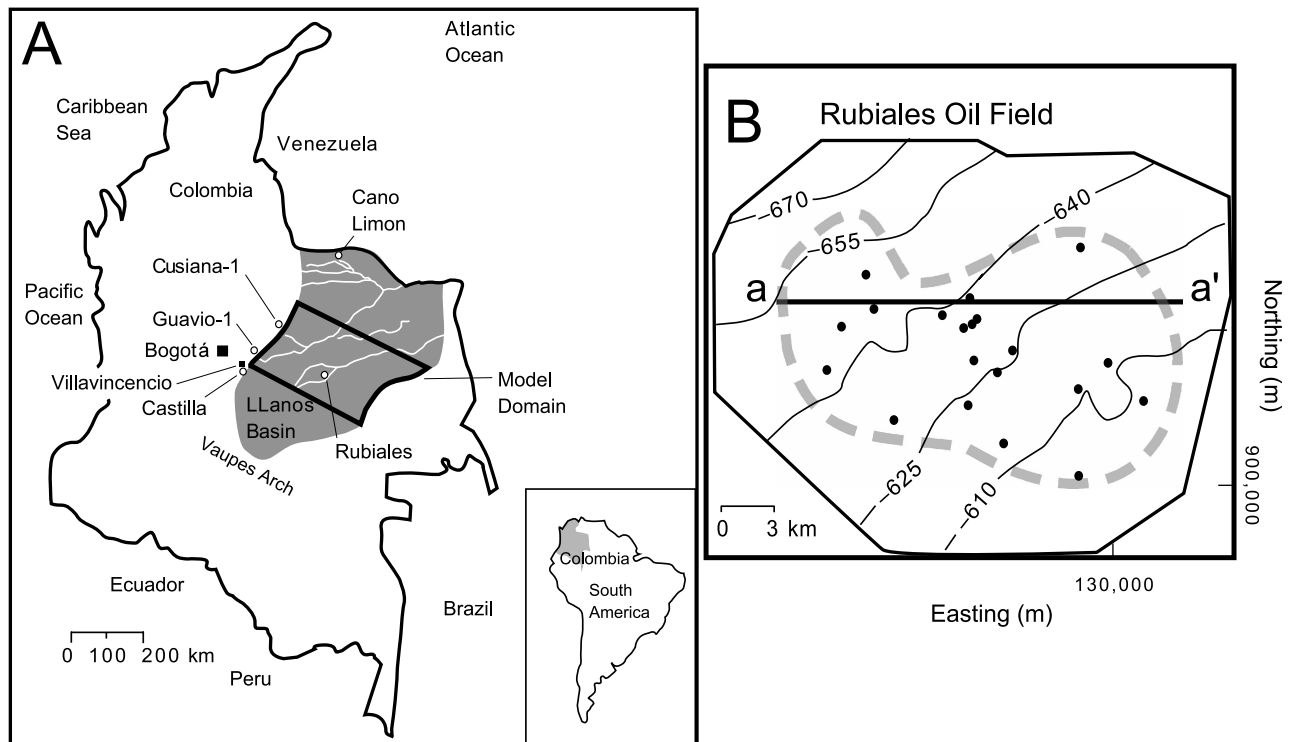


Figure 1. (A) Base map showing Llanos Basin (gray pattern), locations of select oil reservoirs (circles), and surface water drainage patterns (white lines). The location of the Vaupes arch is also shown. (B) The structure at the top of the C7 (black lines) and position of the oil-water contact (dashed line) for the Rubiales oil field (modified from Villegas et al., 1994; Gómez et al., 2009). The grid is in Gauss coordinates.

underpressures can also be formed in recharge areas of regional topography-driven flow systems (Belitz and Bredehoeft, 1988) or because of erosional unloading (Neuzil and Pollock, 1983). Hydraulic heads in the Carbonera Formation (C7 unit) (Figure 3E) vary from subhydrostatic to overpressured (± 400 psi [2.7 MPa] relative to the land surface; Figure 4).

The overpressures near the western margin of the Llanos Basin are likely caused by localized lateral influx of fluids from the higher elevation fold and thrust belt. The observed heads in the C7 unit are higher than local land surface elevation along the western margin of the basin (Figure 3D, E). The C7 head gradients are not oriented parallel to the C7

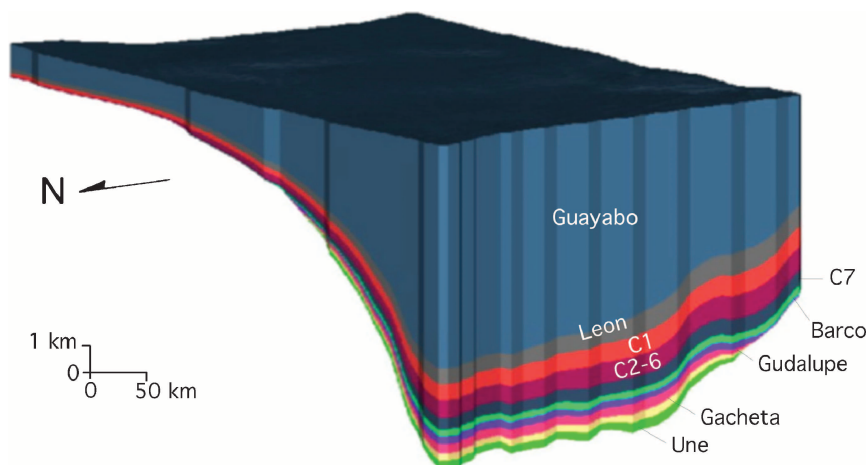
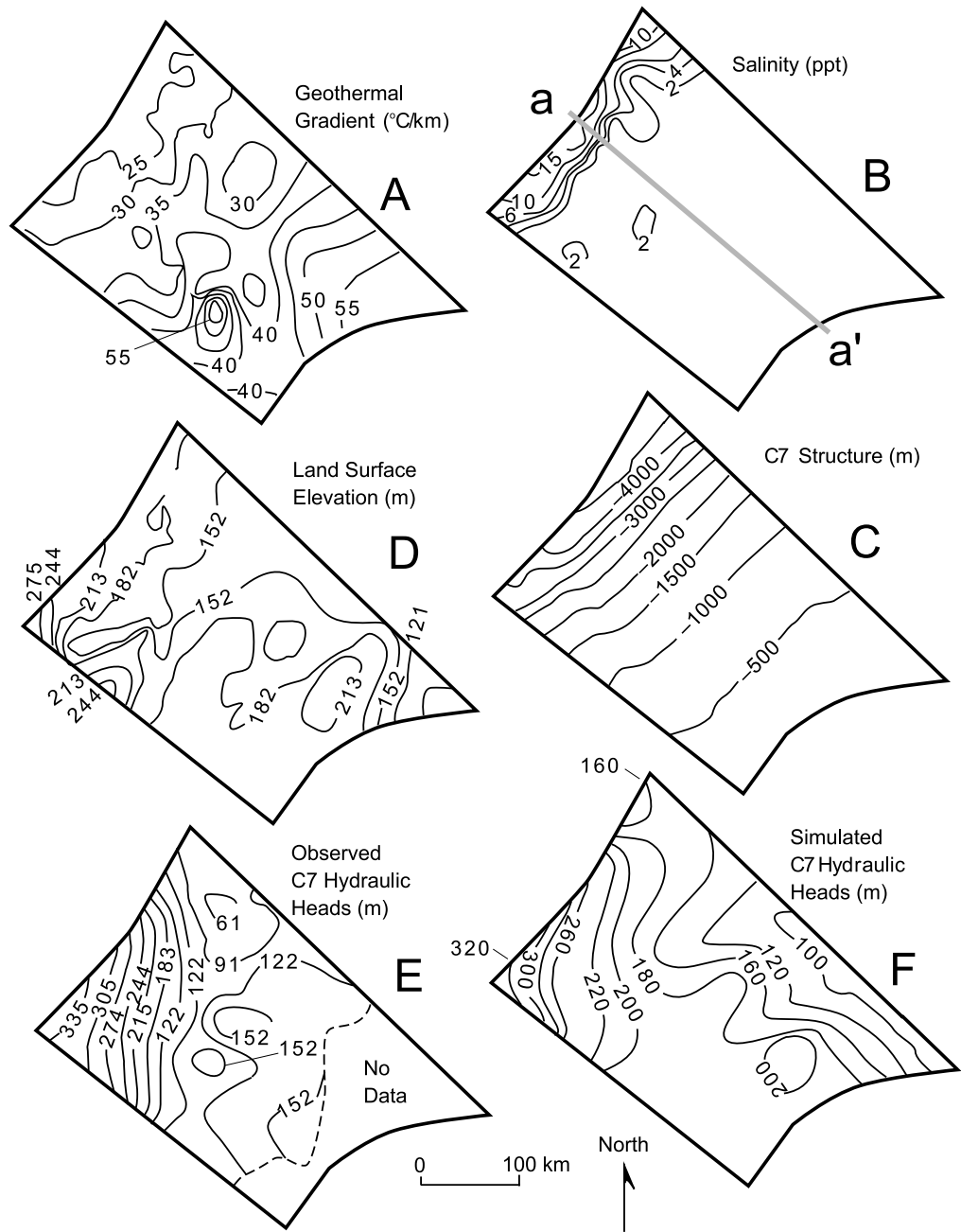


Figure 2. Three-dimensional representation of central Llanos Basin stratigraphy used in the hydrologic model. Vertical exaggeration is 25 \times . The petrophysical properties of each unit in this study are listed in Table 1.

Figure 3. Regional temperature gradients (A; in °C/km), Mirador salinity patterns (B; in ppt), C7 structural slope (C; in m), land surface elevations (D; in m), and observed (E) and computed (F) C7 hydraulic heads (in m) (modified from Villegas et al., 1994). The location of the cross sectional model (aa') is also shown in Figure 3B.



structural slopes across the basin, which could induce a complex secondary oil migration and tilting patterns because of ground-water hydrodynamics.

The main goal of this study was to assess the effect of ground-water hydrodynamics on secondary oil migration within the Llanos Basin at the regional scale using mathematical modeling. Our analysis is limited to the central Llanos Basin where public domain data exist from previous studies (Villegas et al., 1994; Bachu et al., 1995). Although our hydrodynamic analysis is three-

dimensional, we focus on present-day oil migration patterns with the C7 unit. A secondary goal was to better understand the processes controlling anomalous pressure generation, brine flushing, and hydrothermal transport processes within the Llanos Basin. We seek to determine whether pressure, temperature, and salinity anomalies are caused by (1) the presence of an active topography-driven ground-water-flow system (Belitz and Bredehoeft, 1988); (2) variable-density effects associated with high temperatures at depth (Raffensperger and

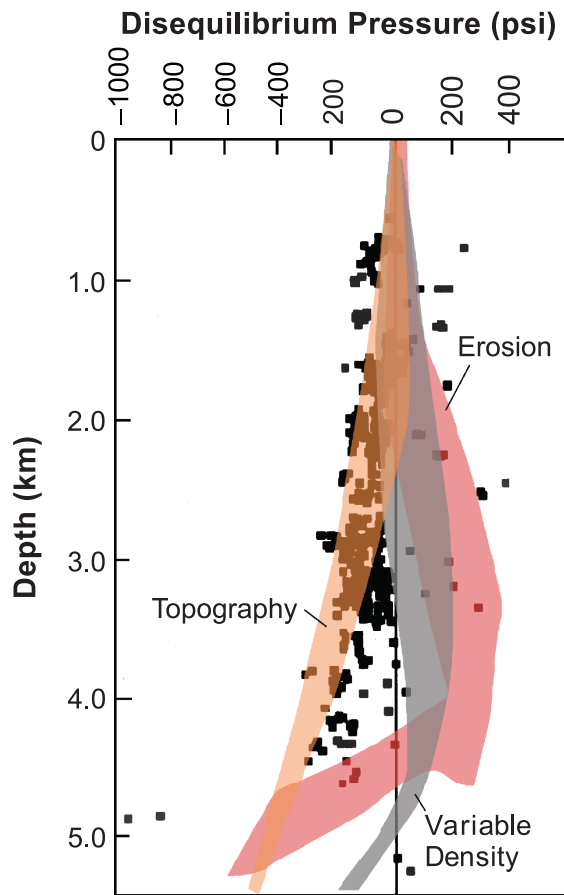


Figure 4. Observed deviatoric fluid pressures within the Llanos Basin, Colombia (Villegas et al., 1994). Also shown are the range of deviatoric pressures from the cross sectional model scenarios, including topography-driven flow (orange patterns), density-driven flow (gray pattern), and erosional unloading (red pattern).

Garven, 1995); or (3) erosional unloading (which would imply a low-permeability environment). These issues are relevant to secondary oil migration because if variable-density effects on fluid flow are significantly affecting ground-water-flow directions, then oil potentials would not accurately reflect ground-water-flow directions.

CONCEPTUAL MODEL

Our analysis of secondary oil migration, presented below, illustrates an exploration strategy for the Llanos Basin and other subaerial-exposed basins that we refer to as the “hydrodynamic stagnation zone” play concept (Figure 5). Hydrodynamic stagnation zones were first proposed by Toth (1988); how-

ever, Toth (1988) presented his hypothesis in the context of horizontal carrier beds having no buoyant drive. The application of the hydrodynamic stagnation zone concept within sloping carrier beds is considered here. A conceptual model of the hydrodynamic stagnation zone hypothesis for sloping reservoirs is presented in Figure 5. In our conceptual model, we consider a sloping reservoir (Figure 5B, E) overlain by a phreatic aquifer with a hummocky water-table topography (Figure 5A, E). These conditions are similar to what is observed in the central and eastern Llanos Basin. Hubbert oil potentials (h_o , Hubbert, 1953; see equation 2 below) for this scenario were calculated using two different oil densities (25 and 45° API; contour lines in Figure 5C, D). Stagnation zones, where oil would accumulate (gray patterns in Figure 5C, D), form adjacent to water table mounds in areas where the structural slopes are relatively gentle. The gradient of Hubbert’s oil potentials, which consider both buoyant and hydrodynamic drives on secondary oil migration, all tilt inward toward the oil potential minimums (where the slope is zero), which is the stagnation zone. Petroleum entering the carrier bed from mature source rocks will migrate down the oil potential slope until it encounters minimums in h_o . Oil that accumulates within a stagnation zone can be sourced from any region where oil migration flow paths terminate in the stagnation zone. We refer to this as the zone of contribution to a hydrodynamic stagnation zone. For relatively heavy oils (25° API) that have little density contrast with ground water, stagnation zones can also form on relatively steep slopes (Figure 5C). We propose here that hydrodynamic stagnation zones arise within the distal parts of the Llanos Basin down gradient from water table mounds. The regions of high hydraulic head drive ground water downdip. As the hydraulic head gradients decay away from the mound and the slope of the bed increases down structural dip, the hydrodynamic effects will diminish. The mounds of high hydraulic head develop because of overlying topographic gradients of the water table aquifer (which is generally considered to be a subdued replica of the land surface) or because of an upflow of overpressured basin fluids along fault zones or erosional

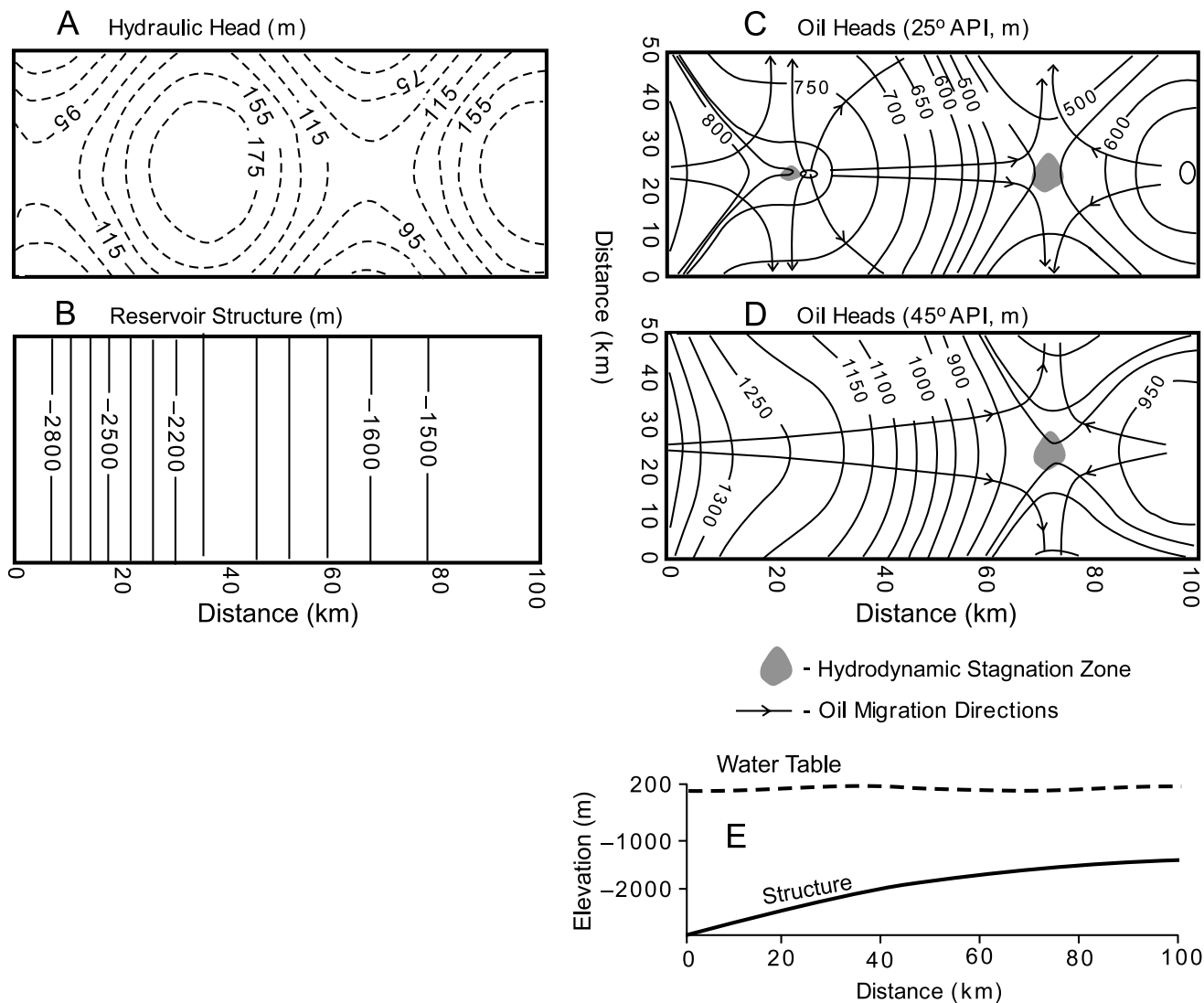


Figure 5. Conceptual model illustrating hydrodynamic stagnation zone play concept. A simple sinusoidal water table profile with a head variation of about 180 m (591 ft) (A) and a monotonic sloping carrier bed (B) were used. Computed Hubbert oil heads (see equation 2) using heavy (C; 25° API) and lighter (D; 45° API) crude oils. A plot of water table and structural slopes along the axis is shown in Figure 5E. The location of the hydrodynamic trap is shown using the gray pattern. We propose that oil will become entrapped down structural gradient from water table mounds. Note that the location of the stagnation zone is not necessarily coincident with the water table minimum or maximum.

gaps in confining units. We demonstrate the viability of this conceptual model by predicting the location of the Rubiales oil field, Llanos Basin.

STUDY AREA

During the Mesozoic and much of the Tertiary, marine conditions prevailed, with a transgressive-regressive transition occurring in the middle of the Llanos Basin (Cooper et al., 1995). Some of the Mesozoic units pinch out to the south and east

(Figure 2). Most of the sediments are characterized by coarse- to fine-grained siliciclastic marine and continental deposits (Table 1). The Mesozoic and Tertiary sections are devoid of significant carbonate or evaporite deposits. Uplift occurred as a result of fold and thrust tectonics on the western margin of the basin beginning in the Miocene. The entire basin became subaerially exposed in the Pliocene during deposition of the Guayabo Formation. The land surface today is gently dipping, with surface topography controlled by river drainage networks that flow to the north-northeast

Table 1. Lithologic Units, Geologic Period, Permeability, and Oil Densities of Select Oil Fields within the Llanos Basin (from Gomez et al., 2009)*

Period	Unit	Perm. (md)	Porosity	Res.	Oil Fields	Lithology
Tertiary	Guayabo	120	0.3			
	Leon	0.12	0.2			
	C1	200	0.2			
	C2-C6	1.16	0.2			
	C7	400	0.3	●	Rubiales (12.6° API)	
	Mirador	375	0.2	●	Cano Limon (29.5° API)	
	Barco/ Los Cuervos	10	0.2			
Cretaceous	Guadalupe	41	0.2			
	Gacheta	140	0.2			
	Une	56	0.2	●	Castilla (19° API)	

*Permeabilities listed in Table 1 were assigned to units in the cross sectional and three-dimensional models. Porosities assigned in three-dimensional models are also listed. Porosity was calculated from an effective stress form of Athy's law for the cross sectional model (see Appendix).

(Figure 1A). The topographic highs occur along the western edge of the basin at about 1300 ft (~396 m) and near the Vaupes arch to the south (and much higher near the city of Villavicencio on the order of 10,000 ft [3048 m]; Figure 1A). Approximately 4 to 6 km (2.5–3.7 mi) of uplift have occurred in the Llanos foothills and basin near the fold and thrust belt.

Oil was first discovered in 1960 in the Llanos foothills (Guavio 1, 532 bbl oil/day [BOPD]). Exploration during the 1970s was mostly unsuccessful. However, in 1983, Triton Energy Corporation drilled a successful well (Cusiana 1) that produced 6500 BOPD. The Rubiales field was discovered in 1982, with production beginning in 1988. In 2010,

the Rubiales field produced about 21,500 BOPD (Cortes et al., 2010) of heavy oil. With the discovery of the Cusiana and Cupiagua fields in 1991 and 1993, respectively, proven reserves for the Llanos Basin grew to more than 2.5 billion bbl of oil (Cazier et al., 1995; Villamil et al., 2004). A recent discovery in the Llanos foothills includes the Gibraltar field with proven reserves of more than 15 million bbl of oil (Villamil et al., 2004).

Petroleum is sourced from a variety of shale units, including the Cretaceous Gacheta and Tertiary Carbonera (C6) and Leon formations. Pyrolysis experiments conducted on Llanos Basin source rocks yield between 6 and 10 mg HC/g kerogen with HC indexes ranging between 300 and 400

(Moretti et al., 2009). Maturation of Llanos Basin source rocks likely began during the Miocene. Maturity varies from overmature within the deepest part of the western Llanos Basin for Cretaceous source rocks to undermature for the shallow-buried Tertiary source rocks in the center of the basin (Moretti et al., 2009). Carbon isotopic analysis of reservoir oils indicates a variety of Tertiary and Cretaceous source rocks (Cortes et al., 2010).

Oil production is from the Cretaceous and Tertiary sandstones, including the Une, Guadalupe, Mirador, and Carbonera formations (Cazier et al., 1995; Villamil et al., 2004; Ramon and Fajardo, 2006; Moretti et al., 2009). Some of these reservoirs (e.g., Cusiana) are noted for their relatively low porosity (8%) but high permeability (>1000 md) (Warren and Pulham, 2002). Many of the largest fields (e.g., Cusiana, Gibraltar, and Cupiana) are located in the Llanos foothills in the western Llanos Basin in anticlinal structures formed by compressional tectonics (Dengo and Covey, 1993; Cazier et al., 1995; Ramon and Fajardo, 2006). Thrust faults likely act as barriers to oil migration and ground-water flow. To the east, normal faults, which cut Tertiary units, can act to trap oil (Moretti et al., 2009). Small fields are generally associated with smaller throws (Moretti et al., 2009).

Oils found in Llanos Basin reservoirs have a variety of sources and levels of biodegradation (Moretti et al., 2009). Heavy oils are found from the Cretaceous Une Formation up through the Tertiary Carbonera reservoir units (C7) (Table 1). As a general rule, low (e.g., Gibraltar, 57° API) to intermediate (e.g., Cusiana, 27–45° API) (Cazier et al., 1995) oil densities are found in the Llanos foothills, indicating limited water washing. Heavy oils are found to the east at shallower depths, suggesting more extensive water washing and biodegradation (e.g., Rubiales, 12° API) (Gómez et al., 2009). Moretti et al. (2009) argue that oils that arrived in a structure early in the history of the Llanos Basin are more likely to be water washed, whereas recently charged oils are still light.

Thermal gradients near the fold and thrust belt are generally low (20°C/km; Figure 3A) but increase to 50°C/km toward the southeastern margin of the basin (Bachu et al., 1995). This is consistent

with the existence of advective heat transfer effects associated with a topographically driven flow system, as documented in other foreland basins (e.g., Ravenhurst et al., 1994). These spatial temperature gradients could influence the depth and timing of oil generation (Person and Garven, 1992).

METHODS

We developed both cross sectional and three-dimensional models of ground-water flow for the Llanos Basin. Motivation for developing cross sectional models was to assess the mechanisms responsible for the underpressures and overpressures reported by Villegas et al. (1994) near the fold and thrust belt. A second goal of the cross sectional models was to determine whether the range of permeability data reported by Villegas et al. (1994) and used in this study could produce ground-water flow systems vigorous enough to flush seawater from marine reservoir units and account for heat-flow anomalies. This calibration exercise provided partial validation for using those same permeability data in our three-dimensional analysis of secondary oil migration. The cross sectional model used here can efficiently represent transport processes such as heat flow and brine migration at the sedimentary basin scale through geologic time (Person et al., 1996). Cross sectional models, however, are not very useful in predicting the location of oil entrapment because oil migration is restricted to the section line. Three-dimensional models are required for this.

Cross Sectional Models of Fluid Flow, Heat, and Solute Transport

The governing transport equations for the cross sectional model are described in the Appendix. The transport equations are solved using the finite element method. The cross sectional model can consider constant-density or variable-density ground-water flow, heat, and solute transport. Underpressures can also be generated in our model by erosional unloading (Corbet and Bethke, 1992). We imposed a specified head condition for fluid flow along the top boundary equal to the water table elevation.

Table 2. Transport Properties Used in the Cross Sectional Model*

Variable	Symbol	Value/Units
Land surface porosity	ϕ	0.3
Irreducible porosity	ϕ_{ir}	0.05
Reservoir sediment compressibility	β	$10^{-9}/\text{Pa}$
Confining unit sediment compressibility	β	$10^{-8}/\text{Pa}$
Specific storage	S_s	$10^{-5}/\text{m}$
Thermal conductivity of fluid	λ_s	0.58 W-m/ $^{\circ}\text{C}$
Thermal conductivity of solids	λ_s	2.5 W-m/ $^{\circ}\text{C}$
Heat capacity of fluid phase	c_f	1000 J/kg
Heat capacity of solid phases	c_s	250 J/kg
Longitudinal dispersivity	α_L	1.0 m
Transverse dispersivity	α_T	0.1 m
Solute diffusivity	D_d	$10^{-10} \text{ m}^2/\text{s}$

*See Appendix for further discussion of these variables.

All other boundaries are no flow. An initial hydrostatic head was assigned to all nodes below the water table. A specified temperature was imposed along the land surface (10°C), and a heat flux of $60 \text{ mW}/\text{m}^2$ was specified along the base of the basin. Sides were assumed to be insulated. We imposed a vertical temperature gradient of $30^{\circ}\text{C}/\text{km}$. For solute transport, the concentration of the water table was set at zero. A vertical salinity gradient was used to assign initial solute concentrations, such that seawater values were reached for Cretaceous marine units at depth. The bottom and side boundaries were treated as no flux. The model was run for 1 m.y., allowing temperatures and salinities to adjust to the ground-water-flow system. The permeabilities assigned to different stratigraphic units in the model are listed in Table 1. Values of parameters that were assumed to be constant for all lithologic units such as thermal conductivity, solute dispersivities, and sediment compressibilities are listed in Table 2.

Three-Dimensional Models of Secondary Oil Migration

To quantify secondary oil migration under hydrodynamic conditions, we also developed a three-dimensional model (Harbaugh et al., 2000) of constant-density ground-water flow for the Llanos

Basin. This approach neglects capillary forces and multiphase flow dynamics considered in reservoir simulators (England et al., 1987). However, these models are typically not used at the sedimentary basin scale because of computational issues and lack of high-quality data regarding permeability heterogeneity.

The governing three-dimensional ground-water-flow equation is given by

$$\frac{\partial}{\partial x} \left[K_h \frac{\partial h}{\partial x} \right] + \frac{\partial}{\partial y} \left[K_h \frac{\partial h}{\partial y} \right] + \frac{\partial}{\partial z} \left[K_z \frac{\partial h}{\partial z} \right] = S_s \frac{\partial h}{\partial t} \quad (1)$$

where h = hydraulic head; K_h = hydraulic conductivity parallel to bedding; K_z = hydraulic conductivity perpendicular to bedding; ρ_f = water density; μ_f = water viscosity; g = gravitational constant; S_s = specific storage (m^{-1}); t = time; x, y, z = spatial dimensions. Our three-dimensional analysis neglects the effects of variable-density flow that could be important in the deepest parts of the Llanos Basin (Villegas et al., 1994; Bachu, 1995). Based on our cross sectional model results, we feel that this approach is valid especially for the shallow regions of the C7 reservoir. The model may not be valid in the deepest regions of the Llanos Basin. The three-dimensional model is intended to evaluate the effects of ground-water flow on long-range oil migration and tilting of oil-water contacts. The three-dimensional model results were compared with reports of entrapped oil within the C7 reservoir (Keeley and Arevalo, 1994).

The computed hydraulic heads extracted from the three-dimensional model were used to calculate oil heads (Hubbert, 1953) in the C7 unit. This approach has been used by numerous previous studies within the Williston Basin (Berg et al., 1994), Alberta Basin (Bekele et al., 2002), Illinois Basin (Bethke et al., 1991), Pannonian Basin (Toth, 2003), Los Angeles Basin (Hayba and Bethke, 1995), and Paris Basin (Bekele et al., 1997). Secondary oil migration within porous, permeable reservoir rocks is generally assumed to be controlled by structural slope and fluid-density differences between oil and formation waters. However, in continental terrains, hydraulic-head gradients induced

by flowing ground water can also influence oil migration patterns, oil entrapment, and the slope of the oil-water interface within a structural trap. In some instances, ground water can flush oil out of petroleum traps. These effects can be quantified using Hubbert's oil potential (Hubbert, 1953):

$$h_{oil} = \frac{\rho_f}{\rho_{oil}} h - \frac{\rho_f - \rho_{oil}}{\rho_{oil}} z_t \quad (2)$$

where h_{oil} = Hubbert's oil head (Hubbert, 1953); h = hydraulic head (Hubbert, 1940); ρ_f = water density; ρ_{oil} = oil density; z_t = elevation of the top of the reservoir. The first term on the right side of equation 2 represents the effects of ground-water flow on oil migration, whereas the second term represents buoyancy effects. Gradients in h and z_t determine oil migration directions. Using typical values of oil and water density (e.g., $\rho_{oil} = 850 \text{ kg/m}^3$ and $\rho_f = 1000 \text{ kg/m}^3$) reveals that the hydrodynamic gradient (hydrodynamic effects) has about seven times greater effect on oil migration than the structural slope (i.e., buoyant forces). This is sometimes referred to as the amplification factor. In this study, we used two oil densities (850 and 980 kg/m^3 ; 35 and 12° API, respectively) to quantify hydrodynamic effects on secondary oil migration for heavy and more typical Llanos Basin oils. We used a water density of 1000 kg/m^3 .

In the three-dimensional model, we computed ground-water velocity vectors as follows:

$$\begin{aligned} q_x^f &= -k_h \frac{\rho_f g}{\mu_f} \frac{\partial h}{\partial x} \\ q_y^f &= -k_h \frac{\rho_f g}{\mu_f} \frac{\partial h}{\partial y} \end{aligned} \quad (3)$$

where k_h = permeability parallel to bedding (note that $K_h = \frac{\rho_f g k_h}{\mu_f}$); μ_f = viscosity of water; g = gravity; ρ_f = density of the water; q_x^f and q_y^f = components of Darcy flux for ground water in the x and y directions. In this study, we assume that no lateral anisotropy in permeability exists.

The gradient in oil potential or oil head (h_{oil}) describes the trajectory of an oil globule or ganglia of petroleum moving through an aquifer in which ground water is flowing. However, other factors

such as relative permeability and capillary pressures can also influence oil velocities and migration directions. We assume here that oil migrates along the top of a carrier bed, neglecting capillary forces and relative permeability effects. In essence, we assume that oil fully saturates the top of the reservoir in which it is flowing. We then can use a form of Darcy's law similar to equation 3 to estimate oil migration directions (Bethke et al., 1991):

$$\begin{aligned} q_x^{oil} &= -k_h \frac{\rho_{oil} g}{\mu_{oil}} \frac{\partial h_{oil}}{\partial x} \\ q_y^{oil} &= -k_h \frac{\rho_{oil} g}{\mu_{oil}} \frac{\partial h_{oil}}{\partial y} \end{aligned} \quad (4)$$

where k = permeability parallel to bedding; μ_{oil} = viscosity of oil; ρ_{oil} = density of oil; q_x^{oil} and q_y^{oil} = components of oil migration in the x and y directions. Equation 4 is only applicable to coarse-grained porous reservoir rocks. If liquid HCs encounter fine-grained heterogeneities within the carrier bed, equation 4 will not accurately represent oil migration directions.

We developed a three-dimensional model using the petrophysical properties shown in Table 1 and stratigraphy in Figure 2. The three-dimensional stratigraphy was derived from east-west and north-south cross sectional profiles presented by Villegas et al. (1994). Strata were allowed to pinch out if the layer thickness was less than 5 m (<16.4 ft). Permeability and porosity were taken mostly from representative values reported by Villegas et al. (1994) (Table 1). In some instances, we chose the minimum reported values for confining units and average values for the reservoirs. We used a horizontal to vertical permeability anisotropy ratio of 100:1 for all units. Porosity decreases with depth, consistent with reported data (Villegas et al., 1994).

The three-dimensional model was composed of 100 rows of nodes in the x and y directions and 10 vertical layers in the vertical. Some lumping of stratigraphic units was done (C2–C6 units; Table 1) because of the lack of field data against which to calibrate properties of individual layers. All of the three-dimensional model simulations were run in a steady-state mode. The three-dimensional model did not represent Paleozoic units that were included in the cross sectional model. We assigned specified heads along the western and northwestern boundaries of the model domain within the

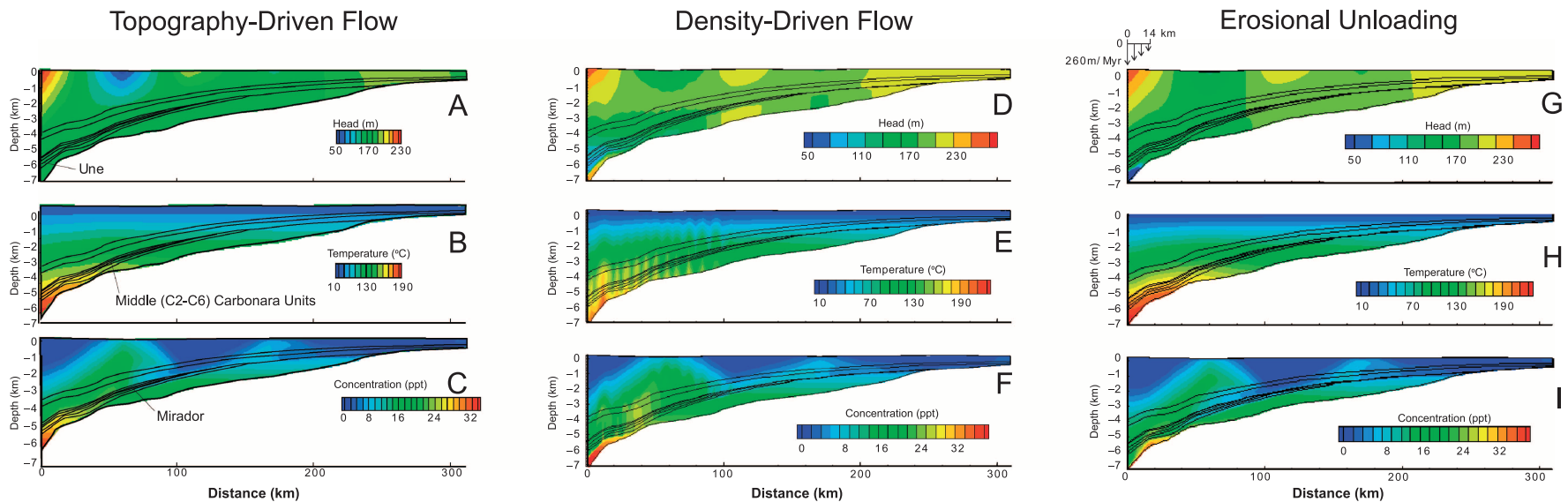


Figure 6. Computed heads (A; in m), temperatures (B; in °C), and salinity patterns (C; in ppt) for the cross sectional model that considers only topography-driven ground-water flow. Computed heads (D; in m), temperatures (E; in °C), and salinity patterns (F; in ppt) for a cross sectional model that considers both topography-driven and variable-density ground-water flow. Computed heads (G; in m), temperatures (H; in °C), and salinity patterns (I; in ppt) for the cross sectional model that considers both topography- and density-driven ground-water flow as well as erosional unloading. The rock properties used in this model are presented in Table 1. The location of the cross section is shown in Figure 3B. Paleozoic rocks included in this model had a permeability of 0.1 md (lowest unit in C).

Mirador-Guadalupe and Une formations to represent lateral inflow from the southwest Llanos Basin and Llanos fold and thrust belt, where heads are higher. Note that the observed heads are higher than land surface elevations along the western margin of the basin (compare panels D and E of Figure 3). In the uplands, the water table was treated as a specified recharge boundary condition that ranged from 0.004 to 0.007 m/day, representing 10 to 50% of precipitation. We included major rivers (Caranpeo, Meta, Tomo, and Muco rivers) as fixed head boundaries; lower order tributaries were not included.

RESULTS

Cross Sectional Model Results

Three cross sectional models are presented to assess the possible mechanisms controlling underpressure formation, brine flushing, and anomalous thermal gradients. The first model represents topography-driven ground-water flow with no erosional unloading and no variable-density effects (Figure 6A–C). Computed underpressures are caused by hydrodynamic effects associated with a regional topography-driven flow system (Belitz and Bredehoeft, 1988). A second simulation (Figure 6D–F) also includes the effects of fluid-density variations associated with thermal and salinity patterns. Underpressures in this model can also form from warm, relatively fresh ground water at depth. A third model is presented that includes underpressure generation associated with up to 240 m (787 ft) of erosional unloading during a 1-m.y. period (Figure 6G–I). Underpressure formation occurs in this simulation because of decompaction as sediments are removed (Corbet and Bethke, 1992). Erosion was imposed along the western basin margin near the fold and thrust belt. All of these models were run for 1 m.y., which we hypothesize is the time period over which modern topographic configuration of the basin pertains. We extracted the salinity patterns for the Mirador as well as shallow thermal gradients for calibration purposes. The permeability of all units was varied by two orders of magnitude in a sensitivity study

(not shown). We found that setting the permeability lower than what is reported here (Table 1) resulted in entrapment of saline pore waters at depth and little change in shallow vertical temperature gradients. Setting the permeability one to two orders of magnitude higher resulted in too much flushing and unrealistically low shallow temperature gradients.

For all model scenarios, we found that ground-water flow was driven primarily by water table gradients at shallow depths (<4 km [<2.4 mi]; Figure 6). For the topography-driven flow simulation, computed heads at depth resulted in underpressures up to 400 psi (2.7 MPa; orange pattern, Figure 4). For the variable-density simulation, some thermal convection cells formed in the deepest part of the Llanos Basin to the west (Figure 6E). These convection cells modified salinity conditions (Figure 6F) but did not seem to have much effect on computed shallow thermal gradients (Figure 7A). For the variable-density simulation shown in Figure 6D, computed heads were as low as 80 m (263 ft)

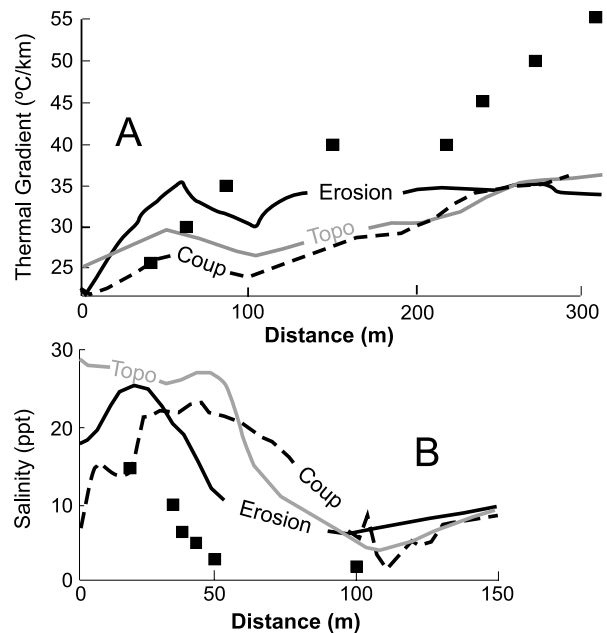


Figure 7. Comparison of computed (lines) and observed (squares) thermal gradients (A; in $^{\circ}\text{C}/\text{km}$) and Mirador salinity patterns (B; in ppt). The gray line denotes the cross sectional model that only considers topography-driven ground-water flow (Topo). The dashed line denotes cross sectional model results that consider both topography- and density-driven flow (Coup). The erosional unloading model is denoted by the solid black line.

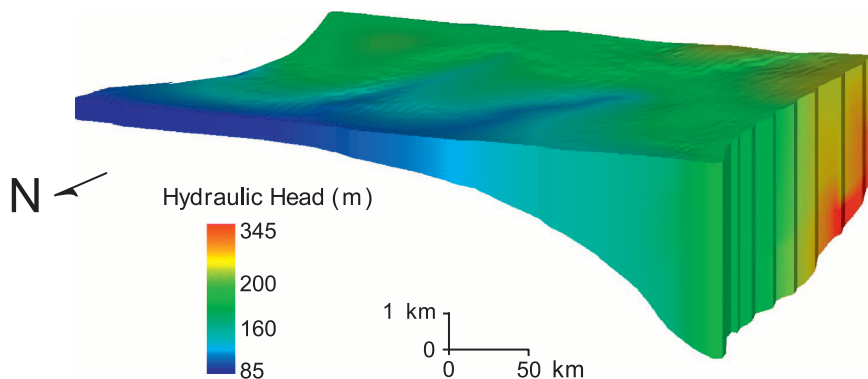


Figure 8. Computed three-dimensional hydraulic heads across the central Llanos Basin. Elevated heads along the western edge of the basin are imposed and represent inflow from the western Llanos Basin ground-water-flow system and adjacent fold and thrust belt.

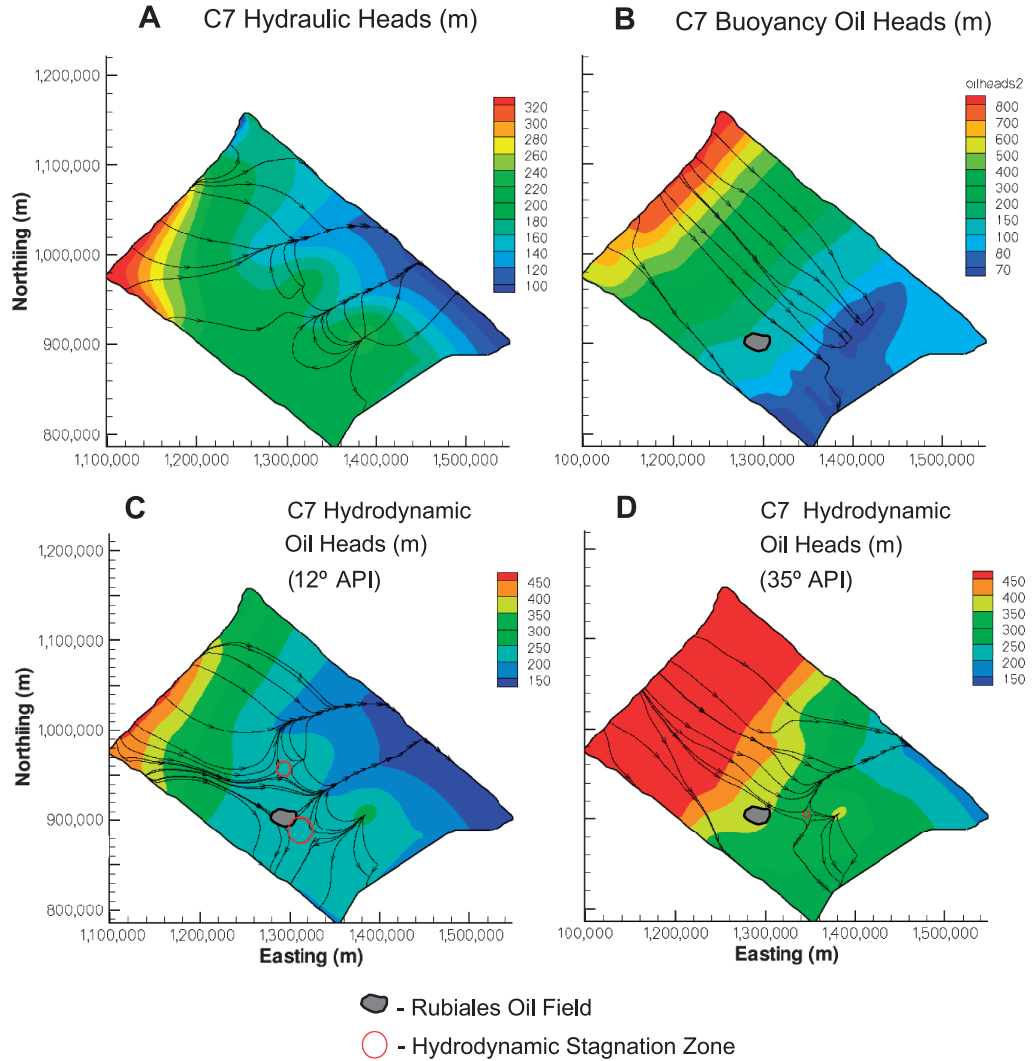
within the Une Formation because of relatively high temperatures (Figure 6E) and brackish salinities (Figure 6F). Computed underpressures were not as low (200 psi [1.37 MPa]; gray pattern, Figure 4). Local thermal convection cells formed within the Cretaceous sand units (Figure 6E) because of the bed thickness and slope (Wood and Hewett, 1984). For the variable-density simulation, computed salinity patterns show alternating high- and low-salinity conditions associated with these convection cells that are not observed in the field data (Figure 7B). For the topography and erosional unloading simulations, the overall trend of decreasing salinity to the east is in reasonable agreement with observed Mirador salinity patterns (Figures 3B, 7B). Salinities are highest within the deepest part of the Mirador Formation (squares, Figure 7B). For the erosional unloading simulation, computed salinity patterns in the Mirador Formation show regions of low salinity where relatively fresh shallow ground water invades (Figure 6I). This is caused, in part, by low heads in the deepest part of the basin (Figure 6G), in combination with the shallow topography-driven flow system induced by hummocky water table topography (Figure 6G). Underpressures from the erosion simulation are as low as 600 psi (4.16 MPa; red pattern, Figure 4). For all models, computed shallow temperature gradients near the fold and thrust belt are as low as 20°C/km (Figure 7A), consistent with field data presented by Bachu et al. (1995). However, for all model scenarios, computed ground-water discharge was not vigorous enough to induce very high temperature gradients (>40°C/km) along the eastern margin of the basin (Figures 6B, E, H; 7A).

Forced thermal convection resulting from shallow flow (<4 km [<2.4 mi] depth) causes low-temperature gradients near the western margin of the basin (Figure 7A). Shallow thermal gradients were as low as 23°C/km to the west. Thermal gradients increase to the east but are not as high as those observed in the field. We conclude that thermal conductivity variations associated with thinning of the sediments to the east, as proposed by Bachu et al. (1995), remains a plausible explanation for the elevated geothermal gradients to the east (50°C/km).

Three-Dimensional Model Results

Permeability values from the cross sectional models (Table 1) were used in the three-dimensional models of ground-water flow and secondary oil migration. Computed head patterns (Figure 8) at depth mostly mimic water table conditions (which closely resemble land surface topography; Figure 3D). To the west, near the fold and thrust belt, high heads imposed along the side boundary of the model domain propagate laterally into the basin. Computed C7 heads (Figures 3F, 9A) are similar, although not identical, in magnitude to the observed conditions (Figure 3B). The simulated C7 heads range from 320 to 100 m (from 1050 to 328 ft). The observed C7 heads range from 335 to 61 m (from 1099 to 200 ft). The overall spatial trends in heads are similar. The lack of agreement in some areas of the C7 reservoir could be due, in part, to permeability heterogeneities not represented in our model and variable-density effects at depth to the northwest. A series of hydraulic head mounds formed in the C7 reservoir in the eastern half of the

Figure 9. Computed C7 hydraulic heads (A; in meters). Buoyancy-driven oil migration is shown in B. Computed oil heads including hydrodynamic effects assuming an oil density of 12 (C; 980 kg/m³) and 35° API (D; 850 kg/m³), respectively. The black lines with arrows represent oil and water migration directions.



basin away from the rivers mimicking land-surface topography (compare Figure 9A or Figure 3F with Figure 3D). Ground-water flow (black lines with arrows in Figure 9) is to the east and north.

Computed oil heads (equation 2) for the C7 reservoir, assuming a water density of 1000 kg/m³ and oil densities of 850 kg/m³ (35° API; Figure 9D) and 980 kg/m³ (12° API; Figure 9C) indicate that ground-water hydrodynamics was an important factor in long-range oil migration and tilting of the present-day oil-water contact in the eastern half of the basin, where the structural slopes are lowest. The slope or tilt of the oil-water contact should mimic oil head gradients, although the absolute elevation of the oil-water contact is determined by the volume of oil in the reservoir. Oil migration directions are indicated by black lines with arrows.

Areas where oil velocities are near zero are indicated by red circles and represent stagnation zones. The gray pattern denotes the location of the Rubiales oil field. Computed oil heads caused by buoyancy alone are presented in Figure 9D. Ground-water flow leads to complex patterns of tilting of the oil-water contact in the eastern Llanos Basin. No single direction of tilting of the oil-water contact exists because of the effects of ground-water flow adjacent to the stagnation zones. For a heavy oil density of 12° API, the Rubiales oil field (gray pattern) is situated within a hydrodynamic stagnation zone (red circles), where oil would be hydrodynamically trapped. A small stagnation zone is also predicted to the north of Rubiales for an oil density of 12° API. The best match between the observed and predicted location of the Rubiales field was found

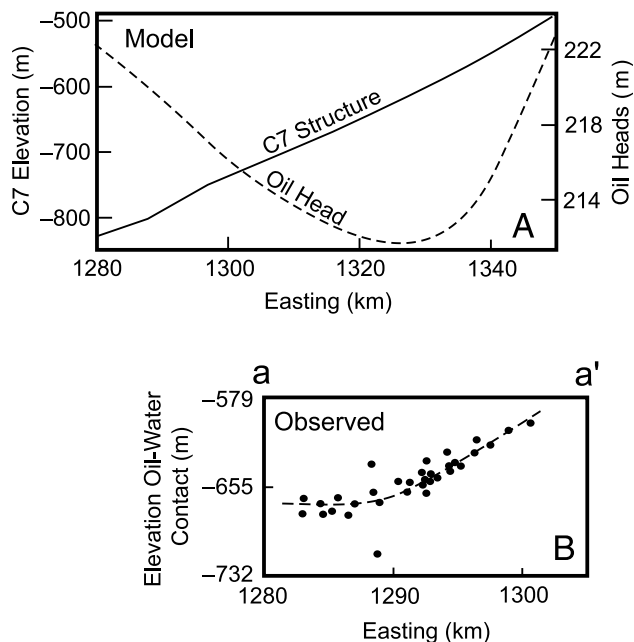


Figure 10. (A) Computed C7 oil heads (dashed line) and C7 structure (solid line) along east-west transect across the southern margin of the Rubiales field. (B) Observed oil-water contact across the Rubiales reservoir (black dots) (from Gómez et al., 2009).

when a heavy oil density of 12° API (980 kg/m³) was used, which suggests that the oil field may have moved as water washing occurred. When a lighter crude is considered (35° API), the position of the stagnation zone shifts to the east of Rubiales (Figure 9C). In both scenarios, the stagnation zone formed in response to the elevated head mound to the east of Rubiales. This mound exists within the observed head map for the C7, although the maximum head is lower (Figure 3E).

Gómez et al. (2009) presented data on oil-water contacts across the Rubiales oil field (Figure 10B). These data suggest that in the downdip part of the field, the oil-water contacts are nearly flat. To the east, the oil water contacts closely match the structural slope. Computed oil heads in the vicinity of the Rubiales oil field (Figure 10A) have a near constant value with slopes dipping inward toward the field to the east and west. The east-west profile of oil head (Figure 10A) was extracted through the center of the computed stagnation zone in Figure 9B. This is more or less consistent with the observed oil-water contact elevation data presented by Gómez et al. (2009).

DISCUSSION

We attempted to show in this study that mathematical models are powerful tools for assessing the validity of the hydrodynamic theory of petroleum entrapment within the Llanos Basin. However, models are not a panacea. We could have learned a great deal about how ground-water flow influenced oil migration directions by simply using the head maps presented by Villegas et al. (1994) for the C7 reservoir and a high-resolution computational grid. Without these head maps, we could not have predicted the potentiometric minimums near the Rubiales field. This suggests that the use of regional pressure or hydraulic head maps is critical to exploration strategies in continental basins with active ground-water-flow systems. One of the main points we learned from the three-dimensional model was that the observed hydraulic head gradients in the shallow Carbonera units are mainly influenced by the overlying water table geometry and lateral leakage of ground water from the Llanos fold and thrust belt. In our view, a more regional quantitative analysis of ground-water flow and oil migration connecting the Llanos fold belt and Llanos Basin is warranted. Basin-scale maps of oil-water contact slope and the degree of water washing would be useful next steps in assessing hydrodynamic effects on oil migration.

The hydrodynamic conditions within the Llanos Basin are probably not so different from other foreland basins along the Eastern Cordillera. Our analysis has shown that ground-water-flow systems cannot be ignored when prospecting for oil in the distal parts of basins where structural slopes are low. The presence of a hydrodynamically entrapped oil field like Rubiales appears to require a water table mound that would cause ground water to flow down a structural gradient. Other Rubiales-type fields may exist within the eastern half of the Llanos Basin down structural gradient from where high potentiometric head mounds occur.

We suspect that much of the anomalous pressures are caused by the presence of a topography-driven flow system, as discussed by Belitz and Bredehoeft (1988). Although density effects cannot be neglected, the natural convection cells shown in

Figure 6 may not exist in nature. By lumping the middle Carbonera units together, we created a thick reservoir that does not occur naturally. Local heterogeneities can strongly influence natural convection cell formation (Gerdes et al., 1995). However, the variable-density analysis was useful in confirming that the shallow C7 flow system is driven primarily by water table topography and justified our use of the constant-density assumption in our secondary oil migration analysis.

The computed oil heads suggest that secondary oil migration within the C7 reservoir along the eastern half of the basin is strongly influenced by ground-water hydrodynamics. Areas with significant brine flushing represent good candidate areas for where hydrodynamic tilting of oil-water contacts may occur. Computed oil heads suggests that the Rubiales oil field appears to be in dynamic equilibrium with its current oil densities.

Finally, note that the models we used had some limitations. Capillary effects caused by sediment facies changes within the C7 reservoir could affect predicted oil migration pathways shown in Figure 9. These were not represented in our model. Faults and fault permeability were not considered in this study. Faults are clearly critical components of oil plays in the Llanos foothills. Accurately representing the position of thrust faults and folded sedimentary packages would be a considerable task for a three-dimensional basin-scale model.

CONCLUSIONS

In this study, we present a new play concept for the Llanos Basin, Colombia, which we refer to as the hydrodynamic stagnation zone play concept. A hydrodynamic stagnation zone is a region having local Hubbert oil potential minimums. We argue that in regions with gentle structural slopes (<1%) and typical water table topographic gradients (~0.5%), ground-water hydrodynamics can create areas where oil is trapped without any need for structural closure. The position of these stagnation zones will also depend on the density contrast between oil and water. Three-dimensional numerical modeling represents a powerful tool to integrate

buoyant and hydrodynamic effects on secondary oil migration in continental terrains.

Cross sectional models were first used to better understand the nature of observed subhydrostatic pressures (400 psi [2.7 MPa]) observed within the western Llanos Basin. We considered three different potential sources of underpressure formation: topography-driven flow, density-driven flow, and erosional unloading. We conclude that the observed underpressures are all likely associated with the presence of a topography-driven ground-water-flow system. Comparison between observed and computed shallow temperature gradients and Mirador salinity trends provided ground truth for our models and allowed us to assess the applicability of published permeability data for reservoirs and seals. Best-fit permeability data from our cross sectional model was used in a three-dimensional analysis of secondary oil migration.

The three-dimensional hydrodynamic model results indicate that hydrodynamic stagnation zones may form in the eastern Llanos Basin as a result of ground-water circulation down structural dip. Hydrodynamic models of secondary oil migration that used relatively heavy oil densities (12° API) predicted the existence of a stagnation zone in the vicinity of the Rubiales oil field. This oil field is enigmatic in that it is located on a monocline with no apparent structural closure.

APPENDIX: CROSS SECTIONAL MODEL TRANSPORT EQUATIONS

We used the cross sectional ground-water-flow model Rift2d (Toupin et al., 1997) in this study. The ground-water-flow equation solved in this study represents the effects of variable-density flow, sea level change, and sediment unloading through time similar to the approach of Bethke and Corbet (1988):

$$\begin{aligned} & \frac{\partial}{\partial x} \left[\frac{k_h \rho_f g}{\mu_o} \mu_r \frac{\partial h}{\partial x} \right] + \frac{\partial}{\partial z} \left[\frac{k_z \rho_f g}{\mu_o} \mu_r \frac{\partial h}{\partial z} \right] \\ & = S_s \left[\frac{\partial h}{\partial t} - \frac{\rho_s - \rho_f}{\rho_f} \frac{\partial L}{\partial t} \right] - \frac{\partial}{\partial z} \left[\frac{k_z \rho_f g}{\mu_o} \rho_r \mu_r z \right] \end{aligned} \quad (5)$$

where k_h and k_z = permeability in the x and z directions, respectively; h = hydraulic head; L = land surface elevation ($\partial L / \partial t$ = erosion or sedimentation rate); g = gravity; z = elevation; ρ_r = relative density (defined below); ρ_s = sediment density; μ_o = fluid viscosity at standard state; μ_r = relative fluid viscosity

(defined below); S_s = specific storage; ρ_f = density of ground water. Equation 5 assumes that the principal directions of permeability (k_h, k_z) are aligned with the x and z axes. Equation 5 further assumes a loading efficiency of 1.0 (i.e., the weight of sediments added or removed from a sedimentary column is transferred to the fluid). This may overestimate induced pore pressure increases and/or decreases by this mechanism at shallow depths (<300 m [<984 ft]). However, at greater depths, a loading efficiency of 1 is probably reasonable. The second term on the right side of equation 5 considers sediment loading and/or unloading. We approximate the total changes in vertical stress using an erosion rate ($\partial L/\partial t$) times a relative sediment-fluid density term. Bredehoeft and Cooley (1983) present a more accurate formulation of the effects of sediment loading and/or unloading on ground water flow, which was not used in this study.

We solved a variable-density form of Darcy's law (Garven and Freeze, 1984) for the specific discharge vector:

$$\begin{aligned} q_x &= -k_h \mu_r \frac{\rho_f g}{\mu_o} \frac{\partial h}{\partial x} \\ q_z &= -k_z \mu_r \frac{\rho_f g}{\mu_o} \left[\frac{\partial h}{\partial z} + \rho_r \right] \end{aligned} \quad (6)$$

where q_x and q_z = Darcy flux in the x and z directions, respectively, for ground water. The relative density (ρ_r) and relative viscosity (μ_r) terms are given by

$$\rho_r = \frac{\rho_f - \rho_o}{\rho_o} \quad (7)$$

$$\mu_r = \frac{\mu_o}{\mu_f} \quad (8)$$

where ρ_o = density of water at the standard state (10°C, salinity of 0.0 mg/L, and atmospheric pressure); μ_o = viscosity of water at standard state; μ_f = viscosity of the fluid at elevated temperature, pressure, and salinity conditions.

Solute Transport

We used a conventional advective and/or dispersive equation to represent time-dependent transport of a conservative solute:

$$\begin{aligned} \phi \frac{\partial C}{\partial t} &= \frac{\partial}{\partial x} \left[\phi D_{xx} \frac{\partial C}{\partial x} + \phi D_{xz} \frac{\partial C}{\partial z} \right] \\ &+ \frac{\partial}{\partial z} \left[\phi D_{zx} \frac{\partial C}{\partial x} + \phi D_{zz} \frac{\partial C}{\partial z} \right] - q_x \frac{\partial C}{\partial x} - q_z \frac{\partial C}{\partial z} \end{aligned} \quad (9)$$

where q_x and q_z = components of the Darcy flux vector in the x and z directions, respectively; ϕ = porosity; D_{xx} , D_{xz} , D_{zx} , and D_{zz} = components of the hydrodynamic dispersion-diffusion tensor (Konikow and Grove, 1977); C = solute concentration (solute mass fraction in kilogram solute per kilogram solution).

Heat Transport

The thickness of the Llanos Basin (up to 5 km [3 mi]) requires that we represent the temperature effects on fluid density. We solved a conductive and convective-dispersive heat transfer equation:

$$\begin{aligned} [c_f \rho_f \phi + c_s \rho_s (1 - \phi)] \frac{\partial T}{\partial t} &= \frac{\partial}{\partial x} \left[\lambda_{xx} \frac{\partial T}{\partial x} + \lambda_{xz} \frac{\partial T}{\partial z} \right] \\ &+ \frac{\partial}{\partial z} \left[\lambda_{zx} \frac{\partial T}{\partial x} + \lambda_{zz} \frac{\partial T}{\partial z} \right] - q_x c_f \rho_f \frac{\partial T}{\partial x} - q_z c_f \rho_f \frac{\partial T}{\partial z} \end{aligned} \quad (10)$$

where λ_{xx} , λ_{xz} , λ_{zx} , and λ_{zz} = components of the thermal dispersion-conduction tensor; T = temperature; c_s and c_f = specific heat capacities of the solid and liquid phases, respectively; ρ_f and ρ_s = density of the fluid and solid phases, respectively. In the model, the thermal dispersion-conduction tensor is a function of the solid thermal conductivity, the fluid thermal conductivity, the porosity, the longitudinal and transverse dispersivities, fluid density, the fluid heat capacity, and the magnitude and direction of the Darcy flux (De Marsily, 1986).

Equation of State

Thermodynamic equations of state are used to compute the density and viscosity of ground water at elevated temperature, pressure, and salinity conditions. We used the polynomial expressions of Kestin et al. (1981):

$$\begin{aligned} \frac{1}{\rho_f} &= a(T) + b(T)P + c(T)P^2 + Cd(T) + C^2e(T) \\ &- PCf(T) - C^2Pg(T) - \frac{h(T)}{2}P^2 \end{aligned} \quad (11)$$

$$\mu_f = \mu_o [1 + B(T, C)P] \quad (12)$$

where $a(T)$, $b(T)$, ..., $h(T)$ and $B(T, C)$ = third- and fourth-order temperature- and concentration-dependent polynomials; P = pressure ($P = [h-z]\rho_f g$). These polynomial expressions are valid for temperatures between 10 and 150°C and salinities between 0 and 6 molal NaCl. Fluid density is less sensitive to changes in fluid pressure than it is to changes in temperature and salinity for the range of conditions encountered in sedimentary basins.

Porosity-Effective Stress Relation

An effective stress form of Athy's law was used to compute porosity changes with depth.

$$\phi = \phi_o \exp[-\beta \sigma_e] + \phi_{ir} \quad (13)$$

where ϕ = porosity; ϕ_o = porosity at the land surface; ϕ_{ir} = irreducible porosity; β = sediment compressibility; σ_e = effective stress (vertical load minus pore pressure).

REFERENCES CITED

- Bachu, S., 1995, Flow of variable-density formation water in deep sloping aquifers: Review of methods of representation with case studies: *Journal of Hydrology*, v. 164, p. 19–28, doi:10.1016/0022-1694(94)02578-Y.
- Bachu, S., J. C. Ramon, M. E. Villegas, and J. R. Underschultz, 1995, Geothermal regime and thermal history of the Llanos Basin, Colombia: *AAPG Bulletin*, v. 79, no. 1, p. 116–129.
- Bekele, E., M. A. Person, and G. De Marsily, 1999, Petroleum migration pathways and charge concentration: A three-dimensional model—Discussion: *AAPG Bulletin*, v. 83, no. 6, p. 1015–1019.
- Bekele, E., M. A. Person, B. J. Rostron, and R. Barnes, 2002, Modeling secondary oil migration with core-scale data: Viking Formation, Alberta Basin: *AAPG Bulletin*, v. 86, no. 1, p. 55–74, doi:10.1306/61EEDA3A-173E-11D7-8645000102C1865D.
- Belitz, K., and J. Bredehoeft, 1988, Hydrodynamics of Denver Basin: Explanation of subnormal fluid pressures: *AAPG Bulletin*, v. 72, no. 11, p. 1334–1359.
- Berg, R. R., W. D. DeMis, and A. R. Mitsdarffer, 1994, Hydrodynamic effects on Mission Canyon (Mississippian) oil accumulations, Billings Nose area, North Dakota: *AAPG Bulletin*, v. 78, p. 501–518.
- Bethke, C., and T. Corbet, 1988, Linear and nonlinear solutions for one-dimensional compaction flow in sedimentary basins: *Water Resources Research*, v. 24, p. 461–467, doi:10.1029/WR024i003p00461.
- Bethke, X. M., J. D. Reed, and D. F. Oltz, 1991, Long-range petroleum migration in the Illinois Basin: *AAPG Bulletin*, v. 75, p. 925–945.
- Bredehoeft, J. D., and R. Cooley, 1983, Comment on: A note on the meaning of the storage coefficient by T. N. Narasimhan and B. Y. Kanehiro: *Water Resources Research*, v. 19, p. 1632–1634, doi:10.1029/WR019i006p01632.
- Cazier, E. C., A. B. Hayward, G. Espinosa, J. Velandia, J.-F. Mugniot, and W. G. Leel Jr., 1995, Petroleum geology of the Cusiana field, Llanos Basin foothills, Colombia: *AAPG Bulletin*, v. 79, no. 10, p. 1444–1463.
- Cooper, M. A., et al., 1995, Basin development and tectonic history of the Llanos Basin, Eastern Cordillera, and middle Magdalena Valley, Colombia: *AAPG Bulletin*, v. 79, p. 1421–1443.
- Corbet, T. F., and C. M. Bethke, 1992, Disequilibrium fluid pressures and groundwater flow in the Western Canada sedimentary basin: *Journal of Geophysical Research*, v. 97, p. 7203–7217.
- Cortes, J., J. Rincon, J. Jaramillo, P. Philp, and J. Allen, 2010, Biomarkers and compound-specific stable carbon isotope of n-alkanes in crude oils from eastern Llanos Basin, Colombia: *Journal of South American Earth Sciences*, v. 29, p. 198–213, doi:10.1016/j.jsames.2009.03.010.
- De Marsily, G., 1986, *Quantitative hydrogeology*: New York, Academic Press, 440 p.
- DeMis, W. D., 1987, Hydrodynamic trapping in Mission Canyon reservoirs: Elkhorn Ranch field, North Dakota, in C. G. Carlson and J. E. Christopher, eds., *Fifth International Williston Basin Symposium: Saskatchewan Geological Society Special Publication 9*, p. 217–225.
- DeMis, W. D., 1995, Effect on cross-basinal hydrodynamic flow on oil accumulations and oil migration history of the Bakken-Madison petroleum system, Williston Basin, North America, in L. D. Vern Hunter and R. A. Schalla, eds., *Seventh International Williston Basin Symposium: 1995 Guidebook*, p. 291–301.
- Dengo, C. A., and M. C. Covey, 1993, Structure of the eastern Cordillera of Colombia: Implications for trap styles and regional tectonics: *AAPG Bulletin*, v. 77, no. 8, p. 1315–1337.
- Eisenberg, L. I., 1993, Hydrodynamic character of the Toro Sandstone, Lagifu-Hedinia area, Aourthne Highlands, Papua New Guinea, in G. J. Carmen and Z. Carmen, eds., *Petroleum exploration and development in Papua New Guinea: Proceedings of the Second Petroleum Convention, Port Moresby, Papua New Guinea*, p. 447–458.
- Eisenberg, L. I., M. V. Vangston, and R. E. Fitzmorris, 1994, Reservoir management in a hydrodynamics environment, Lagifu-Hedinia area, Aourthne Highlands, Papua New Guinea: *Society of Petroleum Engineers Paper 28750*, 18 p.
- England, W. A., A. S. Mackenzie, D. M. Mann, and T. M. Quigley, 1987, The movement and entrapment of petroleum fluids in the subsurface: *Journal of the Geological Society (London)*, v. 144, p. 327–347.
- Garven, G., and R. A. Freeze, 1984, Theoretical analysis of the role of groundwater flow in the genesis of strata-bound ore deposits: 1. Mathematical and numerical model: *American Journal of Science*, v. 284, p. 1085–1124, doi:10.2475/ajs.284.10.1085.
- Gerdes, M., L. Baumgartner, and M. A. Person, 1995, Permeability heterogeneity in metamorphic rocks: Implications from stochastic modeling: *Geology*, v. 23, p. 945–948.
- Gómez, Y., F. Yoris, J. Rodrigues, F. Portillo, and Y. Araujo, 2009, Aspectoshidrodinámicos, estructurales y estratigráficos del Campo Rubiales, Cuenca de los Llanos Orientales, Colombia: *X: Exploración Petroliferaen Cuenecas Sub Andinas, Simposio Bolivariano, Cartagena*, 7 p.
- Harbaugh, A. W., E. R. Banta, M. C. Hill, and McDonald, M. G., 2000, MODFLOW-2000, the U.S. Geological Survey modular ground-water model: User guide to modular concepts and the ground-water flow process: U.S. Geological Survey, Open-File Report 00-92, 121 p.
- Hayba, D., and C. M. Bethke, 1995, Timing and velocity of petroleum migration in the Los Angeles Basin: *Journal of Geology*, v. 103, p. 33–49, doi:10.1086/629720.
- Head, I. M., D. M. Jones, and S. R. Larter, 2003, Biological activity in the deep subsurface and the origin of heavy oil: *Nature*, v. 426, p. 344–352, doi:10.1038/nature02134.
- Howell, V. J., J. Connan, and A. K. Aldridge, 1984, Tentative identification of demethylated tricyclic terpanes in non-biodegraded and slightly biodegraded crude oils from the Los Llanos Basin, Colombia: *Organic Geochemistry*, v. 6, p. 83–92, doi:10.1016/0146-6380(84)90029-9.
- Hubbert, M. K., 1940, Theory of groundwater motion: *Journal of Geology*, v. 48, p. 785–944.

- Hubbert, M. K., 1953, Entrapment of petroleum under hydrodynamic conditions: AAPG Bulletin, v. 37, p. 1954–2026.
- Keeley, M., and E. C. Arevalo, 1994, Colombia-1: Old, new plays may revitalize Colombia's Llanos Basin: Oil & Gas Journal, v. 92, no. 20, p. 66.
- Kestin, J., H. E. Khalifa, and R. Corriea, 1981, Tables of the dynamics and kinematic viscosity of aqueous NaCl solutions in the temperature range of 20–150°C and the pressure range of 0.1–35 MPa: Journal of Physical Chemistry Reference Data, v. 10, p. 71–87.
- Konikow, L. F., and D. B. Grove, 1977, Derivation of equations describing solute transport in groundwater: U.S. Geological Survey Water-Resources Investigations 77-19, 30 p.
- Krieger, F. W., P. J. Eadington, and L. I. Eisenberg, 1996, R_w reserves and timing of oil charge in the Papuan fold belt: Proceedings of the Papua New Guinea Petroleum Convention, v. 3, p. 407–416.
- McIntosh, J. C., and L. M. Walter, 2006, Paleowaters in Silurian–Devonian carbonate aquifers: Geochemical evolution of groundwater in the Great Lakes region since the late Pleistocene: Geochimica et Cosmochimica Acta, v. 70, p. 2454–2479, doi:10.1016/j.gca.2006.02.002.
- Moretti, I., C. Mora, W. Zamora, M. Valendia, M. Mayorga, and G. Rodriguez, 2009, Petroleum system variations in the Llanos Basin (Colombia): Journal of Petroleum Geology, v. 27, no. 4, p. 321–333.
- Neuzil, C., and D. Pollock, 1983, Erosional unloading and fluid pressures in hydraulically “tight” rocks: Journal of Hydrology, v. 91, no. 2, p. 179–193.
- Person, M., and G. Garven, 1992, Hydrologic constraints on petroleum generation within continental rift basins: Theory and application to the Rhine graben: AAPG Bulletin, v. 76, p. 468–488.
- Person, M., J. Raffensperger, G. Garven, and S. Ge, 1996, Basin-scale hydrogeological modeling: Reviews of Geophysics, v. 34, p. 61–87.
- Raffensperger, J. P., and G. Garven, 1995, The formation of uncoformity-type uranium ore deposits I: Coupled groundwater flow and heat transport modeling: American Journal of Science, v. 295, p. 581–636.
- Ramon, J. C., and A. Fajardo, 2006, Sedimentology, sequence stratigraphy, and reservoir architecture of the Eocene Mirador Formation, Cupiagua field, Llanos foothills, Colombia, in P. M. Harris and L. J. Weber, eds., Giant hydrocarbon reservoirs of the world: From rocks to reservoir characterization and modeling: AAPG Memoir 88/SEPM Special Publication, p. 433–469.
- Ravenhurst, C., S. Willett, R. Donelick, and C. Beaumont, 1994, Apatite fission track thermochronometry from central Alberta: Implications for the thermal history of the Western Canada sedimentary basin: Journal of Geophysical Research, v. 99, no. B10, p. 20,023–20,041.
- Schlegel, M. E., Z. Zhou, J. C. McIntosh, C. J. Ballentine, and M. A. Person, 2011, Constraining the timing of microbial methane generation in an organic-rich shale using noble gases, Illinois Basin, U.S.A.: Chemical Geology, v. 287, no. 1–2, p. 27–40, doi:10.1016/j.chemgeo.2011.04.019.
- Toth, J., 1988, Groundwater and hydrocarbon migration, in W. Back, J. S. Rosenshein, and P. R. Sieber, eds., The geology of North America: Hydrogeology: Geological Society of America, v. 0-2, p. 485–502.
- Toth, J., 2003, Fluid-potential patterns and hydrocarbon deposits in groundwater-flow fields induced by gravity and tectonic compression: Hungarian Great Plain, Pannonian Basin: Journal of Geochemical Exploration, v. 78, no. 9, p. 427–431, doi:10.1016/S0375-6742(03)00024-4.
- Toupin, D., M. A. Person, P. Eadington, P. Morin, and D. Warner, 1997, Petroleum hydrogeology of the Cooper and Eromanga basins, Australia: Some insights from mathematical modeling and fluid inclusion data: AAPG Bulletin, v. 81, p. 577–603.
- Villamil, T., et al., 2004, The Gibraltar discovery: Northern Llanos foothills, Colombia: Case history of and exploration success in a frontier area: Journal of Petroleum Geology, v. 27, no. 4, p. 321–333, doi:10.1111/j.1747-5457.2004.tb00061.x.
- Villegas, M., S. Bachu, J. Ramon, and J. Undershultz, 1994, Flow of formation waters in the Cretaceous–Miocene succession of the Llanos Basin, Colombia: AAPG Bulletin, v. 78, no. 12, p. 1843–1862.
- Warren, E. A., and A. J. Pulham, 2002, Anomalous porosity and permeability preservation in deeply buried Tertiary and Mesozoic sandstones in the Cusiana field, Llanos foothills, Colombia: Reply: Journal of Sedimentary Research, v. 72, no. 3, p. 445–448, doi:10.1306/120701720445.
- Wood, J. R., and T. A. Hewett, 1984, Reservoir diagenesis and convective fluid flow, in D. A. McDonald and W. C. Surdam, eds., Clastic diagenesis: AAPG Memoir 27, p. 99–111.
- Zhang, Y., M. Person, and E. Merino, 2005, Hydrologic and geochemical controls on soluble benzene migration in sedimentary basins: Geofluids, v. 5, p. 83–105, doi:10.1111/j.1468-8123.2005.00101.x.